
Effects of Scalar-Tensor-Vector Gravity on relativistic jets

Federico G. Lopez Armengol •
Gustavo E. Romero¹

Abstract Scalar-Tensor-Vector Gravity (STVG) is a theory that does not require dark components to describe astrophysical data. We aim at constraining the free parameters of STVG based on recent observations of the jet in M87. We derive the equations of motion for particles in STVG-Kerr spacetime, we develop a numerical code that integrates such equations, and apply it to the jet of M87. We find that STVG deviates from GR and we set new upper limits for the free parameters of the former. We conclude that STVG is not contradicted by the observational data of M87, and may help to explain jet formation.

Keywords Astrophysical jets, modified gravity

1 Introduction

It has been nearly eighty years since the publication of Babcock (1939) noticing the discrepancies between observed galactic rotation curves and theoretical predictions. Mainstream solutions to this problem have involved the postulation of dark matter. However, every experiment aimed at measuring properties of this kind of matter has failed (Aprile et al. 2012; Akerib et al. 2014; Agnese et al. 2014). In this context, alternative solutions involving modifications of fundamental physical laws deserve some attention.

Milgrom (1983) was the first to account for astrophysical phenomena without dark matter, introducing the Modified Newtonian Dynamics (MOND) the-

ory. In the subsequent years, several relativistic theories whose weak field limit coincides with MOND were formulated. See Famaey and McGaugh (2012) for a review of MOND predictions and its relativistic extensions. Motivated by problems on such extensions, Moffat (2006) postulated the Scalar-Tensor-Vector Gravity theory (STVG), also referred as Modified Gravity (MOG) in the literature.

In STVG, the gravitational coupling constant G is reified to a scalar field whose numerical value exceeds Newton's constant G_N . This assumption serves to correctly describe galaxy rotation curves (Brownstein and Moffat 2006), cluster dynamics (Moffat and Rahvar 2014), and Bullet Cluster phenomena (Brownstein and Moffat 2007), without requiring the existence of dark matter. In order to counteract the enhanced gravitational coupling constant close to the gravitational source, Moffat included a repulsive vector field of short range. In this way, Newton's gravitational constant can be retrieved and STVG coincides with General Relativity (GR), for instance, in the Solar System. The vector field can also mimic the effects of dark matter in the growth of cosmological structures (Shojai et al. 2017). However, according to Jamali and Roshan (2016), any extra field can play the role of dark energy, so the theory still requires a non-vanishing cosmological constant. Further studies of STVG include the gravitational Jeans instability (Roshan and Abbassi 2014), the structure of neutron stars (Lopez Armengol and Romero 2017), the emission of accretion disks around black holes (Pérez et al. 2017), and the stability of galactic disks, where the theory proved to play a similar stabilizing effect as dark matter halos (Ghafourian and Roshan 2017).

The interplay between enhanced attraction and repulsion can be seen from the radial acceleration of a test particle in the weak field, static, spherically symmetric,

Federico G. Lopez Armengol

Gustavo E. Romero

Instituto Argentino de Radioastronomía (CCT-La Plata, CONICET; CICPBA), C.C. No. 5, 1894, Villa Elisa, Argentina

¹Also at Facultad de Ciencias Astronómicas y Geofísicas, Universidad Nacional de La Plata, Paseo del Bosque s/n, 1900 La Plata, Buenos Aires, Argentina.

and constant scalar field approximation (Moffat 2006):

$$a(r) = -\frac{G_N(1+\alpha)M}{r^2} + \frac{G_N\alpha M}{r^2}e^{-m_\phi r}(1+m_\phi r), \quad (1)$$

where M denotes the gravitational mass source, r the distance from it, G_N is Newton's gravitational constant, and α, m_ϕ are free parameters of the theory. The first term in Eq. (1) results in an enhanced attraction, quantified by $G_\infty = G_N(1+\alpha)$, and prevails at $r \rightarrow \infty$. This term describes correctly galaxy rotation curves, light bending phenomena, and cosmological data without dark matter. The second term represents gravitational repulsion and is important when $m_\phi r \ll 1$. This short range force cancels the increase of G_∞ given by α and retrieves G_N as the gravitational coupling constant in the vicinity of the gravitational source.

According to Eq. (1), the differences between STVG and GR manifest far from the gravitational source, where phenomena related to dark matter use to happen. However, we should notice that such equation is based on several assumptions that may fail in the strong field regime.

The purpose of this work is to compare GR and STVG close to the gravitational source, investigate whether they differ on shorter scales as well, and constrain the free parameters of STVG using new high resolution radio observations of the relativistic jet of the nearby galaxy M87. Our objects of study are rotating black holes and the trajectories of test particles close to them.

Actually, we expect peculiar deviations. The repulsive force that counteracts the enhanced attraction is led by a vector field, and vector forces are not restricted to the radial direction; they have azimuthal or polar components instead, like the Lorentz force in Electromagnetism (EM). We expect STVG to predict novel gravitational *Lorentz-like* effects, completely absent in GR.

Relativistic jets, launched from the surroundings of supermassive black holes in active galactic nuclei (AGNs), should be sensitive to such Lorentz-like effects. This is because the launching region is near the event horizon, where the strong field is important, and because of the highly relativistic velocities involved. In the case of nearby sources such effects might be observationally detectable. Particularly, the extragalactic jet of the giant elliptical galaxy M87 (a.k.a Virgo A, NGV4486, and 3C274) has been resolved up to 100 gravitational radii using Very Long Baseline Interferometry (VLBI) (Mertens et al. 2016). This, along with constraints on the size of M87 supermassive black hole (hereafter M87*) from mm-VLBI observations (Broderick et al. 2015), might provide a unique scenario to test some predictions of STVG.

Our work is organized as follows: in Section 2 we present the action and field equations of STVG, along with certain simplifications. In Section 3 we describe STVG-Kerr black hole and spacetime, and derive the equations of motion for test particles. Then, in Section 4 we explain a numerical method developed to integrate such equations for particles in a relativistic jet. Section 5 is devoted to our main results for the case of M87*, and consequent constraints on the free parameters of STVG. In Section 6 we discuss the applicability of the theory to the formation of relativistic jets, and in Section 7 we present our main conclusions.

2 STVG action and field equations

STVG action reads¹:

$$S = S_{\text{GR}} + S_\phi + S_S + S_M, \quad (2)$$

where

$$S_{\text{GR}} = \frac{1}{16\pi} \int d^4x \sqrt{-g} \frac{1}{G} R, \quad (3)$$

$$S_\phi = - \int d^4x \sqrt{-g} \left(\frac{1}{4} B^{\mu\nu} B_{\mu\nu} - \frac{1}{2} m_\phi^2 \phi^\mu \phi_\mu \right), \quad (4)$$

$$S_S = \int d^4x \sqrt{-g} \left[\frac{1}{G^3} \left(\frac{1}{2} g^{\mu\nu} \nabla_\mu G \nabla_\nu G - V(G) \right) + \frac{1}{G m_\phi^2} \left(\frac{1}{2} g^{\mu\nu} \nabla_\mu m_\phi \nabla_\nu m_\phi - V(m_\phi) \right) \right]. \quad (5)$$

Here, $g_{\mu\nu}$ denotes the spacetime metric, R the Ricci scalar, and ∇_μ the covariant derivative; ϕ^μ denotes a Proca-type massive vector field, m_ϕ its mass, and $B_{\mu\nu} = \partial_\mu \phi_\nu - \partial_\nu \phi_\mu$; $V(G)$ and $V(m)$ denote possible potentials for the scalar fields $G(x)$ and $m_\phi(x)$, respectively. We adopt the metric signature $\eta_{\mu\nu} = \text{diag}(-1, 1, 1, 1)$ and natural units. The term S_M in the action refers to possible matter sources.

We take certain simplifications into account: we neglect the mass m_ϕ of the vector field because its effects manifest at kiloparsecs from the source, and our region of interest is contained within sub-parsec scales. Physically, this means that we are not considering the decay of the Yukawa-type force. The same approximation has been made in Moffat (2015); Hussain and Jamil (2015).

¹Compared with the original action in Moffat (2006), we drop the cosmological constant term because its effects are locally negligible. We also ignore the scalar field ω and set the potential $W(\phi) = 0$ as suggested by Moffat and Rahvar (2013); Moffat (2006), respectively.

Further, we approximate the scalar field G as a constant and adopt the same prescription as Moffat (2006):

$$G_\infty = G_N(1 + \alpha), \quad (6)$$

where α is a free parameter whose value we sample.

Lastly, we nullify the matter action term S_M because we study the vacuum spacetime of a rotating black hole.

The simplified action takes the form:

$$S = \int d^4x \sqrt{-g} \left[\frac{1}{16\pi G_\infty} R - \frac{1}{4} B^{\mu\nu} B_{\mu\nu} \right], \quad (7)$$

which formally resembles the Einstein-Maxwell action, and suggests the existence of gravitational Lorentz-like effects in STVG.

By varying the simplified action (7) with respect to the metric $g^{\mu\nu}$ we obtain:

$$G_{\mu\nu} = 8\pi G_\infty T_{\mu\nu}^\phi, \quad (8)$$

where $G_{\mu\nu}$ denotes the Einstein tensor and

$$T_{\mu\nu}^\phi = -\frac{2}{\sqrt{-g}} \frac{\delta S_\phi}{\delta g^{\mu\nu}} = \left(B_\mu^\alpha B_{\nu\alpha} - g_{\mu\nu} \frac{1}{4} B^{\rho\sigma} B_{\rho\sigma} \right). \quad (9)$$

Furthermore, varying the action (7) with respect to the vector field ϕ_μ yields:

$$\nabla_\nu B^{\nu\mu} = 0. \quad (10)$$

Finally, the equations of motion for a test particle in coordinates x^μ are given by:

$$\left(\frac{d^2 x^\mu}{d\tau^2} + \Gamma_{\alpha\beta}^\mu \frac{dx^\alpha}{d\tau} \frac{dx^\beta}{d\tau} \right) = \frac{q}{m} B^\mu{}_\nu \frac{dx^\nu}{d\tau}, \quad (11)$$

where τ denotes the particle proper time, and q the coupling constant with the vector field. We define the parameter:

$$\kappa = \frac{q}{m}, \quad (12)$$

whose value we will sample, along with α .

3 STVG-Kerr spacetime

Moffat (2015) investigated the STVG-Kerr spacetime. This is the vacuum and axially symmetric solution to the metric field equations (8), for a body with mass M

and spin per unit mass a . In Boyer-Lindquist coordinates, it reads:

$$ds^2 = -\frac{\Delta}{\rho^2} \left[d(ct) - \frac{a \sin^2 \theta}{c} d\phi \right]^2 + \frac{\sin^2 \theta}{\rho^2} \left[\left(r^2 + \frac{a^2}{c^2} \right) d\phi - \frac{a}{c} d(ct) \right]^2 + \frac{\rho^2}{\Delta} dr^2 + \rho^2 d\theta^2, \quad (13)$$

where

$$\Delta = r^2 - \frac{2G_\infty M}{c^2} r + \frac{a^2}{c^2} + \frac{G_N Q^2}{c^4}, \quad (14)$$

$$\rho^2 = r^2 + \frac{a^2}{c^2} \cos^2 \theta, \quad (15)$$

$$Q = \sqrt{\alpha G_N M}. \quad (16)$$

The black hole geometry (13) presents two horizons, given by the roots of $\Delta = 0$:

$$r_\pm = \frac{G_\infty M}{c^2} \left(1 \pm \sqrt{1 - \frac{c^2 a^2}{G_\infty^2 M^2} - \frac{\alpha}{1 + \alpha}} \right), \quad (17)$$

and an ergosphere determined by the roots of $g_{00} = 0$:

$$r_E = \frac{G_\infty M}{c^2} \left(1 \pm \sqrt{1 - \frac{c^2 a^2 \cos^2 \theta}{G_\infty^2 M^2} - \frac{\alpha}{1 + \alpha}} \right). \quad (18)$$

Furthermore, the spacetime possesses a ring singularity, given by the roots of $\rho = 0$.

Such geometrical features change with α . In particular, the external event horizon of a rotating black hole in STVG is bigger than in GR. In Section 5 we make use of this fact to constrain the value of α from mm-VLBI observations of M87*.

Having described the STVG-Kerr spacetime, we turn our attention to the vector field ϕ . The vector field equation (10) for the black hole geometry (13) has been studied exhaustively in the context of Einstein-Maxwell theory (see, for instance, Misner et al. (1973)). Adapting such results to STVG, we find:

$$\mathbf{B} = \frac{Q}{c\rho^4} (r^2 - a^2 \cos^2 \theta) \mathbf{dr} \wedge \left[\mathbf{dt} - \frac{a}{c} \sin^2 \theta \mathbf{d}\phi \right] + \frac{2Qa}{c^2 \rho^4} r \cos \theta \sin \theta \mathbf{d}\theta \wedge \left[\left(r^2 + \frac{a^2}{c^2} \right) \mathbf{d}\phi - \frac{a}{c} \mathbf{dt} \right], \quad (19)$$

that corresponds to the vector potential:

$$\phi = -\frac{Qr}{\rho^2} (\mathbf{dt} - a \sin^2 \theta \mathbf{d}\phi). \quad (20)$$

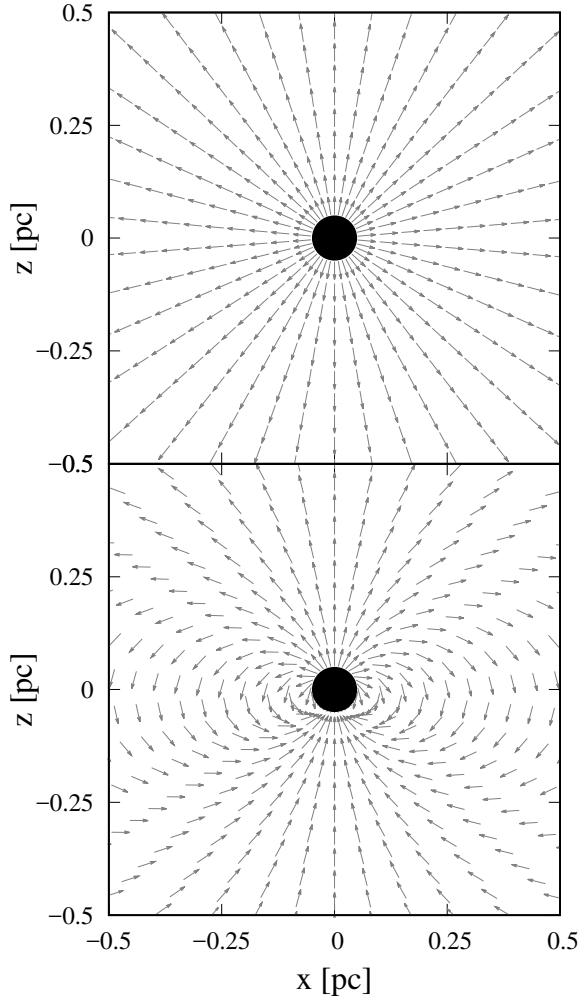


Fig. 1 Vector maps of $B^{\mu\nu}$ on Kerr-Schild $x-z$ plane. The field is generated by a supermassive black hole with mass $M = 6 \times 10^9 M_\odot$, and angular momentum $a = 0.9 G_N M/c$. The field lines are normalized. *Top*: Gravito-electric components B^{0i} . These radial components generate a repulsive force that counteracts the enforced attraction, and retrieves Newton gravitational law on the right scale. *Bottom*: Gravito-magnetic components B^{ij} . The field lines have the familiar disposition of a magnetic dipole generated by a rotating charge. The effects of these components involve novel predictions of STVG

Following Moffat's idea, the *gravito-electrical* components B^{0i} counteract the enhanced attraction. However, *gravito-magnetic* components B^{ij} give raise to azimuthal and polar forces, completely absent in GR. In Fig. 1 we map the latter components.

We then proceed to study the trajectory of a test particle with mass m in STVG-Kerr spacetime. The equations of motion (11), for the geometry (13) and tensor field (19), has been treated in the context of Einstein-Maxwell theory (see Carter (1968); Misner et al. (1973)). Making use of these results, we obtain a system of first order differential equations:

$$\rho^2 \frac{dr}{d\lambda} = \pm \sqrt{R(r)}, \quad (21)$$

$$\rho^2 \frac{d\theta}{d\lambda} = \pm \sqrt{\Theta(\theta)}, \quad (22)$$

$$\rho^2 \frac{d\phi}{d\lambda} = - \left(\frac{aE}{c^2} - \frac{a}{\sin^2 \theta} \right) + \frac{aP(r)}{\Delta(r)c^2}, \quad (23)$$

$$\rho^2 \frac{dt}{d\lambda} = - \frac{a \sin^2 \theta}{c^2} \left(\frac{aE}{c^2} - \frac{L}{\sin^2 \theta} \right) + \left(r^2 + \frac{a^2}{c^2} \right) \frac{P(r)}{\Delta(r)c^2}, \quad (24)$$

where $\lambda = \tau/m$, E stands for the energy of the test particle, and L for its angular momentum around the symmetry axis. Both E and L are constants of motion. Further, we have the functions:

$$R(r) = \frac{P^2(r)}{c^2} - \Delta(r) (m^2 r^2 c^2 + \mathcal{K}), \quad (25)$$

$$\Theta(\theta) = \mathcal{Q} - \cos^2 \theta \left[a^2 \left(m^2 - \frac{E^2}{c^4} \right) + \frac{L^2}{\sin^2 \theta} \right], \quad (26)$$

$$P(r) = E \left(r^2 + \frac{a^2}{c^2} \right) - aL - qQr, \quad (27)$$

where \mathcal{K} is Carter's constant of motion, and \mathcal{Q} a particular combination of constants. We present expressions for the latter in the following section.

4 Numerical treatment

We develop a numerical code that integrates the system of differential equations (21)-(24) for a particle in a relativistic jet. The input variables of the code are observational parameters of the astrophysical jet:

1. We fix the spacetime geometry and fields by setting M , a , and α . The values of α are obtained through the parameter M_0 , studied extensively by Moffat and collaborators (Brownstein and Moffat 2006, 2007). Both parameters are related by:

$$\alpha = \sqrt{\frac{M_0}{M}}. \quad (28)$$

2. We set the intrinsic properties of the particle m , κ , and its initial position (r_0, θ_0, ϕ_0) . Without loss of generality, we set $\phi_0 = 0$.
3. Now we focus on the initial values for $p_\mu = dx_\mu/d\lambda$. Since we are interested in azimuthal effects given by gravito-magnetic forces, we set initially:

$$p_\phi = 0. \quad (29)$$

4. For the t -component, we have:

$$p_t = -mc\gamma\sqrt{g_{tt}}, \quad (30)$$

where γ is the local Lorentz factor of the particle.

5. The initial components p_r , p_θ require further steps because they depend on the ejection angle θ_{ej} between the initial velocity and the z -axis. Since the z -axis is well defined in Kerr-Schild coordinates, first we have to solve the system of non-linear equations for the initial Kerr-Schild momentum components \tilde{p}_x , \tilde{p}_z :

$$\begin{aligned} \cos \theta_{\text{ej}} &= \frac{\tilde{p}^i z^j g_{ij}}{\sqrt{\tilde{p}^i \tilde{p}_i} \sqrt{z^i z_i}} = \\ &= \frac{\tilde{p}^x z^x g_{xx} + \tilde{p}^x z^z g_{xz} + \tilde{p}^z z^z g_{zz}}{\sqrt{(\tilde{p}^x)^2 g_{xx} + 2\tilde{p}^x \tilde{p}^z g_{xz} + (\tilde{p}^z)^2 g_{zz}} \sqrt{g_{zz}}}, \end{aligned} \quad (31)$$

$$\begin{aligned} \tilde{p}^\mu \tilde{p}_\mu &= (p_t)^2 g^{tt} + 2\tilde{p}^x p_t + 2\tilde{p}^z p_t + (\tilde{p}^x)^2 g_{xx} + \\ &+ 2\tilde{p}^x \tilde{p}^z g_{xz} + (\tilde{p}^z)^2 g_{zz} = -m^2 c^2, \end{aligned} \quad (32)$$

- where $z^i = (0, 0, 1)$. We set $\tilde{p}_y = 0$ in consistency with $p_\phi = 0$, and we take p_t from Eq. (30). We solve the non-linear system of equations applying a Newton-Raphson subroutine from Press et al. (1992). After finding the initial components \tilde{p}_x , \tilde{p}_z , we obtain the corresponding Boyer-Lindquist components p_r , p_θ from a direct change of coordinates.
6. With the initial values of p_μ , we calculate the constants of motion:

$$E = -p_t c - qA_t, \quad (33)$$

$$L = p_\phi + qA_\phi, \quad (34)$$

$$\mathcal{K} = p_\theta^2 + \cos^2 \theta \left[a^2 \left(m^2 - \frac{E^2}{c^4} \right) + \frac{L^2}{\sin^2 \theta} \right], \quad (35)$$

and the combination

$$\mathcal{Q} = \mathcal{K} + \left(L - \frac{aE}{c^2} \right)^2. \quad (36)$$

The mass of the particle is the fourth constant of motion, that we calculate as a check for consistency:

$$m = \sqrt{\frac{-p^\mu p_\mu}{c^2}}. \quad (37)$$

7. We proceed to integrate Eqs. (21)-(24) numerically. To that aim, we apply a fourth order Runge-Kutta subroutine.
8. Based on the expression of Crawford and Tereno (2002), we calculate the local Lorentz factor γ as measured by a Zero Angular Momentum Observer $u_\mu \rightarrow (u_t, \vec{0})$.

5 Results

We apply the numerical code described in the previous section to the supermassive black hole in M87. We set $M = 6 \times 10^9 M_\odot$ and $a = 0.9 G_N M / c$, as estimated by Gebhardt et al. (2011) and Li et al. (2009), respectively.

From observations reported by Broderick et al. (2015) we know that the radius of M87* is, at most, $8 G_N M / c^2$. This estimation implies an upper limit for the parameter M_0 and, correspondingly, for α (see Eq. 17):

$$M_0 \lesssim 10^{11} M_\odot. \quad (38)$$

In the first run, we fix $M_0 = 10^{11} M_\odot$ and sample the values $\kappa_1 = 10^2 \sqrt{\alpha G_N}$, $\kappa_2 = 10^3 \sqrt{\alpha G_N}$, and $\kappa_3 = 10^4 \sqrt{\alpha G_N}$, where $\sqrt{\alpha G_N}$ is Moffat's original prescription for κ . We set the mass $m = 1 \text{g}$ and the initial position $r_0 = 140 G_N M / c^2$, $\theta_0 = 0.18$, $\phi_0 = 0$. For the initial Lorentz factor we use $\gamma = 2$. Such parameters are based on recent observational results (Mertens et al. 2016).

We explore different values for the ejection angle: $\theta_{\text{ej}}^A = 0$ and $\theta_{\text{ej}}^B = 0.3$, which we refer as *case A* and *case B*, respectively. In Fig. 2 we show the disposition of the initial velocities, with the local gravito-magnetic field. Because of gravito-magnetic forces, we expect opposite signs in the angular velocity ω_ϕ for each case.

In Fig. 3 we plot ω_ϕ , defined as the ratio between $d\phi/d\lambda$ and $dt/d\lambda$, as a function of z . We find significant deviations from GR. In case A, rotation along ϕ is enhanced by gravito-magnetic forces, leading to higher maxima. On the contrary, for case B, we obtain negative values for ω_ϕ . This is because gravito-magnetic forces are now directed towards $-\phi$.

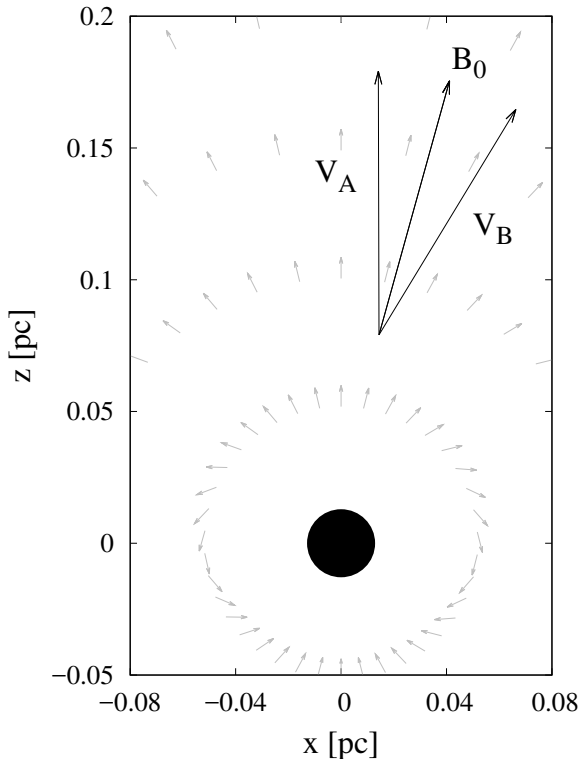


Fig. 2 Initial disposition of the velocities of particles for cases A and B with respect to the initial gravito-magnetic field line. Because of gravito-magnetic forces, we expect opposite signs for the angular velocity ω_ϕ .

Along the trajectories, the gravito-magnetic field lines rotate and change their disposition with respect to the velocity of the particle. Then, even for case B, ω_ϕ grows for larger z . This can be seen in Fig. 4 where we plot the $x-z$ trajectories for both cases, along with gravito-magnetic field lines. The filled region in the latter figure is the relativistic jet of M87*, with opening angle $\Theta \sim 0.18$ (Mertens et al. 2016).

The enhanced gravito-electrical repulsion by growing κ affects significantly the kinematic properties of the test particle. In Fig. 5 we see that the local Lorentz factor γ grows with time and reaches high values. Then, in the strong field regime of STVG, particles gravitationally accelerate. The energy source for such acceleration is the potential energy term of Eq. (33). This can be used to invoke an active role of gravity in the acceleration of the jet.

However, there are observational constraints on the velocities of the inner jet of M87. The highest value of γ estimated by Mertens et al. (2016) corresponds to the spine of the jet and is $\gamma \sim 10$. Then, based on Fig. 5, we state the upper limit:

$$\kappa \leq 10^2 \sqrt{\alpha G_N}. \quad (39)$$

From Fig. 4 we can also notice the effects of gravito-electric and magnetic forces deflecting particles in θ . The repulsive gravito-electric forces accelerate particles in the radial direction, moving them away from the rotational axis in case A. On the contrary, particles move towards the rotational axis in case B. This effect is also facilitated by gravito-magnetic forces since, for instance in case A, when particles acquire positive angular velocity ω_ϕ , a second order gravito-magnetic force is generated in the polar direction. This results in the motion of particles away from the rotational axis. On the other hand, for particles in case B with negative ω_ϕ , the second order gravito-magnetic force is directed towards the rotational axis. Through this effect, gravito-magnetic forces could considerably contribute to collimation at the base of the jet, since gravito-magnetic field lines are almost vertical there.

Now, in a second run, we sample $M_0 = 10^{10} M_\odot$, $10^{11} M_\odot$ and $10^{12} M_\odot$. The latter violates restriction (38) but we include it for consistency checks. Such values for M_0 imply the approximate values $\alpha \approx 4$, 13, and 40. Notice that, within this values, is included $\alpha \sim 9$ as determined by Moffat and Rahvar (2013) and frequently used in references. We take Moffat's weak field limit prescription $\kappa = \sqrt{\alpha G_N}$, and we set $\theta_{ej} = 0$, i. e. particles are ejected along the axis z .

We find Lorentz-like forces to be negligible and we associate this fact to the small value of κ . The trajectories, indeed, are almost indistinguishable. However,

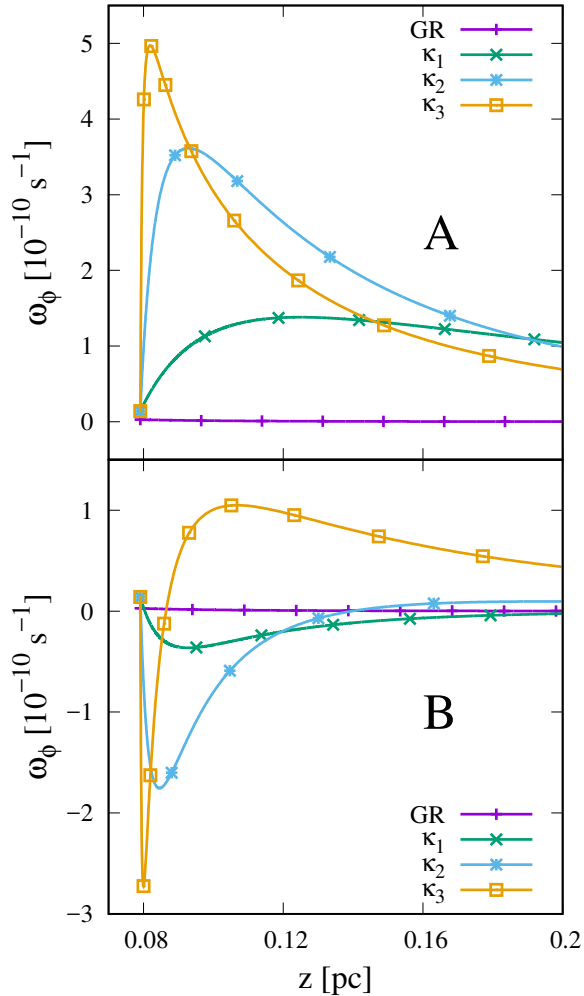


Fig. 3 *Top:* Angular velocity ω_ϕ as a function of z for case A. Maxima grows with κ as a consequence of the increase of gravito-magnetic forces. Rapid decay happens because particles deviate in θ and get aligned with the field lines, nullifying gravito-magnetic forces. *Bottom:* Angular velocity ω_ϕ as a function of z for case B. Initially, ω_ϕ is negative due to gravito-magnetic forces. Such forces are absent in GR, where $\omega_\phi > 0$ due to frame dragging effects. The subsequent behavior of ω_ϕ is related to the disposition of gravito-magnetic field lines and the velocity of the particles along the trajectory.

we find large deviations on kinematic properties. In Fig. 6 we plot the local Lorentz factor γ as a function of time, and find that the decrement is greater for larger α . Then, although with Moffat’s prescription for κ repulsion and attraction grow in equal proportion, attraction prevails because the dependence of curvature with α is highly non-linear.

All these results show that STVG theory has an important impact on the physics of relativistic jets. In the next section, we discuss some interesting applications to jet phenomenology.

6 Discussion

We have studied the trajectories of particles in STVG-Kerr spacetime. We found that STVG is not equivalent to GR in the strong field regime. In the face of current problems on the models of jet formation, some STVG predictions seem attractive.

The case of M87 and its jet is particularly interesting since the jet has been recently resolved on scales of 100-1000 Schwarzschild radii (Mertens et al. 2016). Very Long Base Line radio observations at 43 GHz have revealed a jet that initially expands with a parabolic profile (Asada and Nakamura 2012) and then transits to a conical jet at a projected distance of ~ 350 mas ($2 \text{ mas} \approx 0.16 \text{ pc}$). The radius of the jet evolves with the distance to the central source as $r_{\text{jet}} \propto z^{0.6}$, with significant oscillations that might reflect the growing of Kelvin-Helmholtz instabilities. The observations revealed the existence of a structured jet with clear stratification: a slow outer component and a faster relativistic spine (Mertens et al. 2016).

The jet of M87 is the first one where rotation has been directly observed. The jet first rotates clockwise and then the outer components rotates counterclockwise. Assuming conservation of the specific energy and angular momentum, and assuming Keplerian motion in the accretion disks, a rotation angular velocity of $\omega_\phi \sim 10^{-6} \text{ s}^{-1}$ is obtained (Mertens et al. 2016).

At the launching region, the effects of gravito-magnetic forces of STVG are critical. Then, we conjecture that the observed rotation might result from gravitational forces. In order to check the viability of this conjecture, we run our code adopting $r_0 = 5R_S$, $M_0 = 10^{10}M_\odot$, $\kappa_1 = 10^1\sqrt{\alpha G_N}$, $\kappa_2 = 10^2\sqrt{\alpha G_N}$, $\kappa_3 = 10^3\sqrt{\alpha G_N}$, and a wide ejection angle, as expected from the Blandford-Payne mechanism for jet launching (Blandford and Payne 1982; Spruit 2010). The $x - z$ trajectories obtained for different values of κ are shown in Fig. 7. The filled region in the latter figure is the jet, as parametrized by Mertens et al. (2016) on this scale.

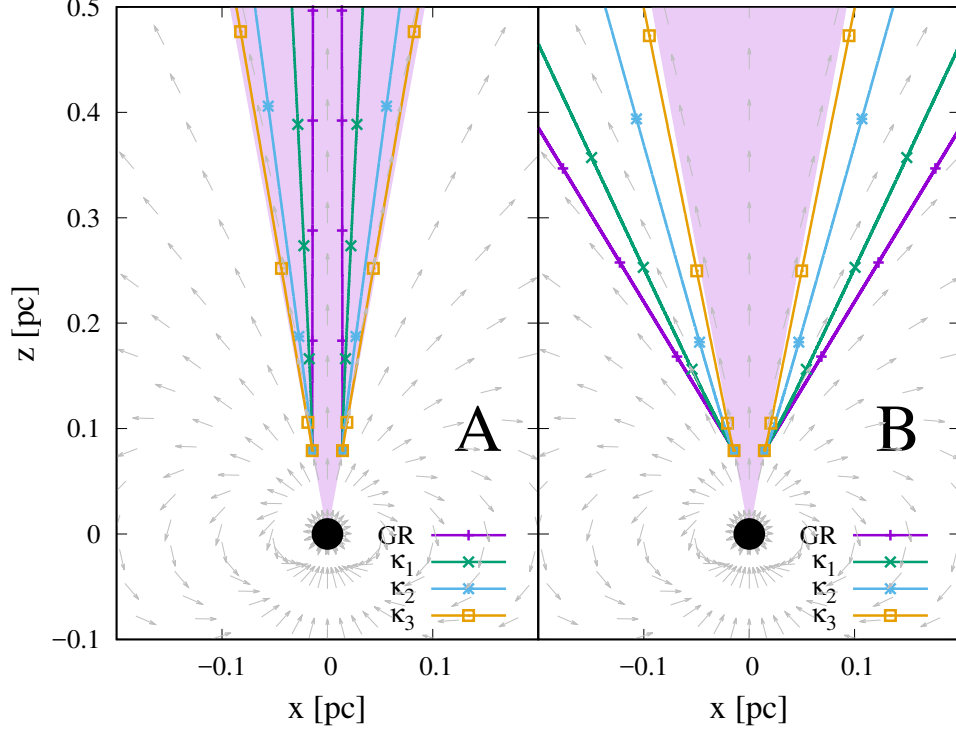


Fig. 4 *Left:* $x - z$ projection of trajectories for distinct values of κ , for particles initially ejected along z (case A). Gravitomagnetic forces leads to deflection in θ . *Right:* $x - z$ projection of trajectories for distinct values of κ , with initial ejection angle $\theta_{\text{ej}}^{\text{B}} = 0.3$ (case B). Gravitomagnetic forces contribute to jet collimation, deviating the particle towards the rotation axis. The filled regions represent the sub-parsec relativistic jet of M87.

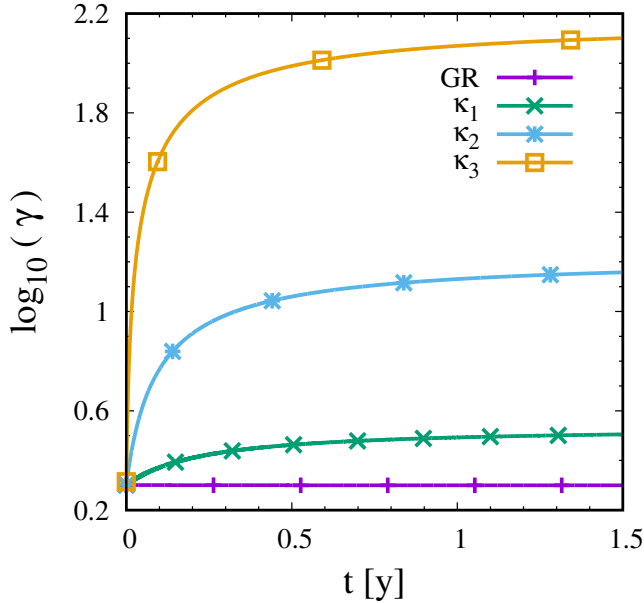


Fig. 5 Local Lorentz factor γ for particles in case A as a function of t for different values of κ . The enhancement of repulsive gravito-electric forces with κ leads to growing γ , i.e. particles are gravitationally accelerating. We make use of this fact to state an upper limit for κ . Particles in case B present similar behaviors for γ .

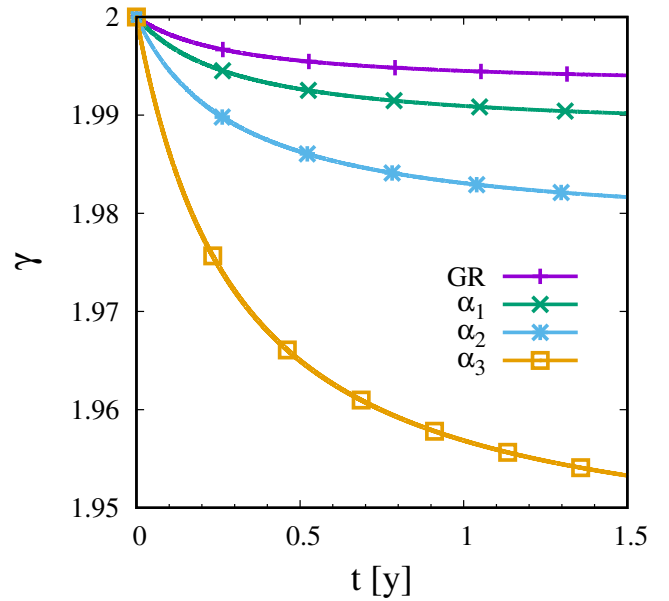


Fig. 6 Local Lorentz factor γ for different values of α , as a function of t . Although Moffat's prescription for κ reproduce GR predictions in the Solar System, we can see that this is not the case in the strong field regime. The dependence of curvature with α is highly non-linear, and the values of γ decrease deeper for larger α .

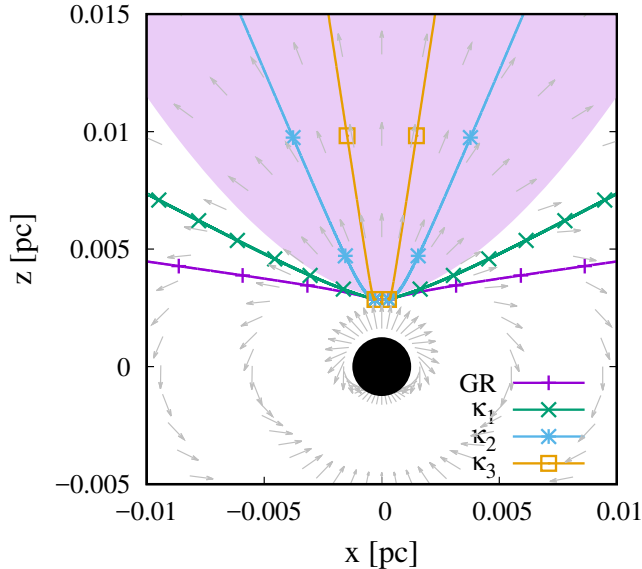


Fig. 7 $x - z$ projection of trajectories, for different values of κ , at the launching region of the jet. The filled region is the jet in M87, as parametrized by Mertens et al. (2016). Gravitomagnetic forces contribute to the collimation of the jet.

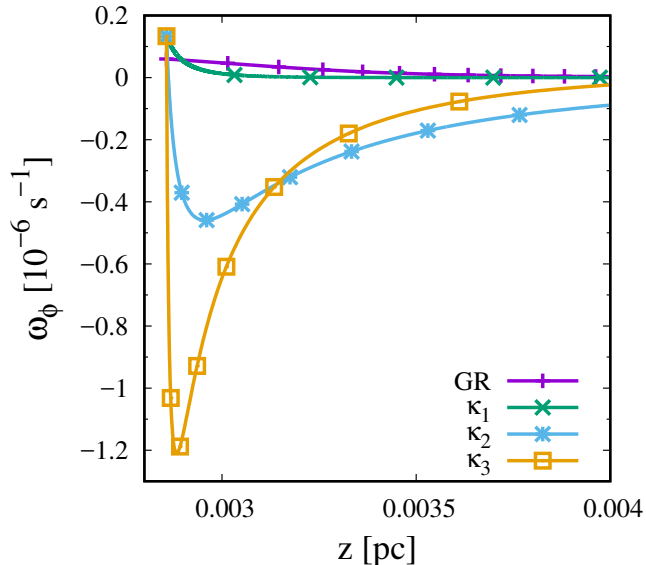


Fig. 8 Angular velocity ω_ϕ for particles ejected with a wide angle, at the launching region of the jet. The behavior of ω_ϕ is related to the disposition of gravitomagnetic field lines and the velocity of the particles along the trajectory. These effects are absent in GR, where particles rotate due to frame-dragging effects.

We notice the effects of gravito-magnetic and electric forces contributing to the collimation of the jet.

In Fig. 8 we plot the angular velocity ω_ϕ as a function of z , for different values of κ . We can see that the initial gravito-magnetic force leads to counter-rotation in ϕ . But, as we mentioned in the previous section, the field lines rotate along the trajectory and, from a given z , the sign of gravito-magnetic forces change and ω_ϕ starts growing. The scale where jet rotation gets inverted, and the order of magnitude for ω_ϕ , are consistent with the observational results and the phenomenological modeling of Mertens et al. (2016).

The standard magnetic model for jet formation has contradictory conditions for strong jet collimation and strong acceleration, since they require distinct inclination angles for the magnetic field lines. It is usually argued that collimation might be produced by some external agent. For instance, Spruit et al. (1997) propose a collimation mechanism based on a dipole-like magnetic field. Since the gravito-magnetic field of STVG is independent of the standard magnetic field, it may serve as such external agent as well.

Our discussion suggests that gravity, through STVG, may play an important role in the formation of astrophysical jets. We should mention, however, that similar statements have been made for GR. For instance, de Felice and Calvani (1972) studied the allowed ranges of variation for the coordinate θ in the geodesics of Kerr spacetime. They found a set of geodesics for unbound particles, which they called *vortical orbits*, that spiral around the symmetry axis and never cross the equatorial plane. Further, de Felice and Curir (1992) showed that perturbing particular vortical orbits leads to collimation around the symmetry axis.

In order to find out whether STVG is more adequate than GR to model jet formation, we analyze the amount of vortical orbits in STVG-Kerr spacetime. We adapt the conditions de Felice and Calvani (1972) for vortical orbits to the modified equation of motion (22) and find:

$$\Gamma > 0, \quad (40)$$

$$-a^2\Gamma \leq \mathcal{Q} + L^2 \leq a^2\Gamma, \quad (41)$$

$$L^2 + \mathcal{Q} \leq L^2 \leq \frac{(a^2\Gamma + L^2 + \mathcal{Q})^2}{4a^2\Gamma}, \quad (42)$$

where $\Gamma = E^2/c^4 - m^2$. We vary the initial angle θ_0 , and the ejection angle θ_{ej} , and test whether the resulting trajectories satisfy the latter vortical conditions.

In Fig. 9 we plot the parameter space $\theta_0 - \theta_{ej}$, and fill the regions that include vortical orbits. As we can see, the number of vortical orbits grows with κ . This occurs because gravito-magnetic forces led to better collimation and gravito-electrical repulsion enhances radial ac-

celeration. Future work will be devoted to the analysis and perturbation of such orbits.

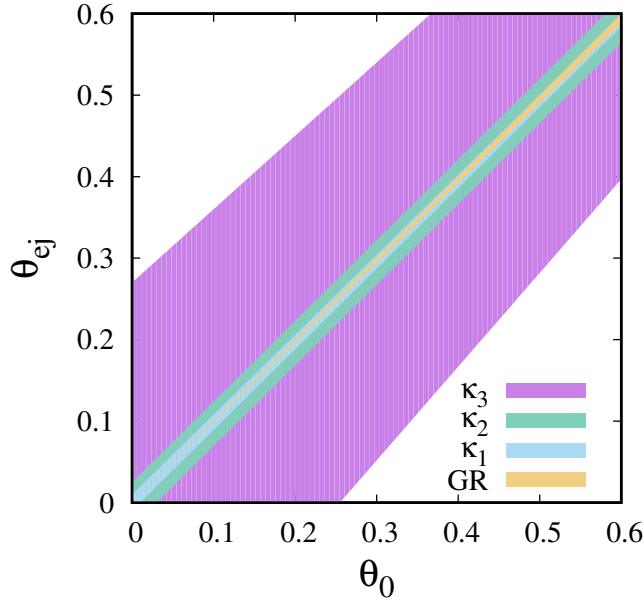


Fig. 9 Parameter space $\theta_0 - \theta_{ej}$, where regions of vortical orbits has been filled. STVG includes a larger amount of vortical orbits for growing κ , as compared to GR. Therefore, STVG seems more suitable for explaining jet formation.

7 Conclusions

We applied STVG theory to the black hole and jet in M87. We followed Moffat's prescription and approximated the scalar field G as a constant. Also, we approximated $m_\phi = 0$ because its effects manifest at kiloparsec scales, and we were interested on sub-parsec structures. We found resemblances of this regime with Einstein-Maxwell formalism.

We described STVG-Kerr spacetime. The black hole event horizon and ergosphere grow in size with the free parameter α . Since there are constraints on the size of M87* from mm-VLBI observations, we set an upper limit for the related parameter M_0 of the theory.

Unlike many gravitational theories, STVG is not purely geometrical. Instead, it includes a Yukawa-type vector field ϕ that couples to matter. We characterized the effects of such vector field on the motion of particles in STVG-Kerr spacetime. Repulsive gravito-electrical components counteracts enhanced attraction and serves to recover classical limits, while gravito-magnetic components involve novel predictions of STVG.

We derived the equations of motion for test particles in STVG-Kerr spacetime. Such equations depend on the coupling constant κ . Moffat proposed the value

$\kappa = \sqrt{\alpha G_N}$ for recovering classical limits, but this prescription only works on the weak field regime. Instead, we treated κ as a free parameter, and study its effects on particle motion.

We developed a code that integrates the trajectories of particles in a relativistic jet, and used it to model the jet in M87. First, we used the code to sample the parameter κ . The effects of gravito-magnetic forces arose and the theory clearly deviates from GR. Because of gravito-electrical repulsion, we found that particles gravitationally accelerate and reach high Lorentz factors. Based on observational constraints for velocities in the relativistic jet of M87, we determined an upper limit for κ in our model. On the other hand, gravito-magnetic forces influenced the angular velocity ω_ϕ , depending critically on the ejection angle. As a third effect, we found collimation and de-collimation in the coordinate θ , also depending on the initial ejection angle.

Then, we sampled α , adopting the prescription of Moffat for the parameter κ . The effects of Lorentz-like forces on trajectories resulted negligible. However, the increase of the energy of the black hole with α led to a larger decrease of the particle velocity, as compared with GR.

From both runs, we concluded that STVG differs with GR not only far from the gravitational source, where phenomena associated with dark matter use to happen, but also in the strong field regime.

We compared observational results on the formation zone of the jet in M87 with predictions of STVG. We concluded that gravity, through STVG, might play an important role in the process of acceleration and collimation of the jet. This conclusion is supported by the analysis of vortical orbits in STVG. Interestingly enough, we found that the observed rotation and counter-rotation of the jet in M87 could be a consequence of the gravito-magnetic field.

Acknowledgements This work was supported by grants AYA2016-76012-C3-1-P (Ministro de Educación, Cultura y Deporte, España) and PIP 0338 (CONICET, Argentina). We would like to thank Luciano Combi and Santiago del Palacio for helpful discussions.

References

- Agnese, R., *et al.*: Physical Review Letters **112**(24), 241302 (2014). doi:10.1103/PhysRevLett.112.241302
- Akerib, D.S., *et al.*: Physical Review Letters **112**(9), 091303 (2014). doi:10.1103/PhysRevLett.112.091303
- Aprile, E., *et al.*: Physical Review Letters **109**(18), 181301 (2012). doi:10.1103/PhysRevLett.109.181301
- Asada, K., Nakamura, M.: Astrophysical Journal Letters **745**, 28 (2012). doi:10.1088/2041-8205/745/2/L28
- Babcock, H.W.: Lick Observatory Bulletin **19**, 41 (1939). doi:10.5479/ADS/bib/1939LicOB.19.41B
- Blandford, R.D., Payne, D.G.: Mon. Not. R. Astron. Soc. **199**, 883 (1982). doi:10.1093/mnras/199.4.883
- Broderick, A.E., Narayan, R., Kormendy, J., Perlman, E.S., Rieke, M.J., Doeleman, S.S.: The Astrophysical Journal **805**, 179 (2015). doi:10.1088/0004-637X/805/2/179
- Brownstein, J.R., Moffat, J.W.: Astrophys. J. **636**, 721 (2006). doi:10.1086/498208
- Brownstein, J.R., Moffat, J.W.: Mon. Not. R. Astron. Soc. **382**, 29 (2007). doi:10.1111/j.1365-2966.2007.12275.x
- Carter, B.: Physical Review **174**, 1559 (1968). doi:10.1103/PhysRev.174.1559
- Crawford, P., Tereno, I.: General Relativity and Gravitation **34**, 2075 (2002). doi:10.1023/A:1021131401034
- de Felice, F., Calvani, M.: Nuovo Cimento B Serie **10**, 447 (1972)
- de Felice, F., Curir, A.: Classical and Quantum Gravity **9**, 1303 (1992). doi:10.1088/0264-9381/9/5/012
- Famaey, B., McGaugh, S.S.: Living Reviews in Relativity **15**, 10 (2012). doi:10.12942/lrr-2012-10
- Gebhardt, K., Adams, J., Richstone, D., Lauer, T.R., Faber, S.M., Gültekin, K., Murphy, J., Tremaine, S.: The Astrophysical Journal **729**, 119 (2011). doi:10.1088/0004-637X/729/2/119
- Ghafourian, N., Roshan, M.: Mon. Not. R. Astron. Soc. **468**, 4450 (2017). doi:10.1093/mnras/stx661
- Hussain, S., Jamil, M.: Phys. Rev. D **92**(4), 043008 (2015). doi:10.1103/PhysRevD.92.043008
- Jamali, S., Roshan, M.: Eur. Phys. J. **C76**(9), 490 (2016). 1608.06251. doi:10.1140/epjc/s10052-016-4336-x
- Li, Y.R., Yuan, Y.F., Wang, J.M., Wang, J.C., Zhang, S.: The Astrophysical Journal **699**(1), 513 (2009)
- Lopez Armengol, F.G., Romero, G.E.: General Relativity and Gravitation **49**, 27 (2017). doi:10.1007/s10714-017-2184-0
- Mertens, F., Lobanov, A.P., Walker, R.C., Hardee, P.E.: Astronomy and Astrophysics **595**, 54 (2016). doi:10.1051/0004-6361/201628829
- Milgrom, M.: The Astrophysical Journal **270**, 365 (1983). doi:10.1086/161130
- Misner, C.W., Thorne, K.S., Wheeler, J.A.: Gravitation. W. H. Freeman, San Francisco (1973)
- Moffat, J.W.: J. Cosmol. Astropart. Phys. **3**, 004 (2006). doi:10.1088/1475-7516/2006/03/004
- Moffat, J.W.: European Physical Journal C **75**, 175 (2015). doi:10.1140/epjc/s10052-015-3405-x
- Moffat, J.W., Rahvar, S.: Mon. Not. R. Astron. Soc. **436**, 1439 (2013). doi:10.1093/mnras/stt1670
- Moffat, J.W., Rahvar, S.: Mon. Not. R. Astron. Soc. **441**, 3724 (2014). doi:10.1093/mnras/stu855
- Pérez, D., Armengol, F.G.L., Romero, G.E.: Phys. Rev. D **95**(10), 104047 (2017). doi:10.1103/PhysRevD.95.104047
- Press, W.H., Teukolsky, S.A., Vetterling, W.T., Flannery, B.P.: Numerical Recipes in Fortran 77: The Art of Scientific Computing, 2nd edn. Cambridge University Press, Cambridge (1992)
- Roshan, M., Abbassi, S.: Phys. Rev. D **90**(4), 044010 (2014). doi:10.1103/PhysRevD.90.044010
- Shojai, F., Cheraghchi, S., Bouzari Nezhad, H.: Physics Letters B **770**, 43 (2017). doi:10.1016/j.physletb.2017.04.029
- Spruit, H.C.: In: Belloni, T. (ed.) Lecture Notes in Physics, vol. 794. Berlin Springer Verlag, Berlin Heidelberg (2010). doi:10.1007/978-3-540-76937-8-9
- Spruit, H.C., Foglizzo, T., Stehle, R.: Mon. Not. R. Astron. Soc. **288**, 333 (1997). doi:10.1093/mnras/288.2.333
-